Pulsatile flow dynamics determine pulmonary arterial architecture

Stephen Spurgin,[1,2] Lauren Thai,[2] Tina Wan,[3,4] Christopher P. Chaney,[5] Mitzy A. Cowdin,[1] Suren V. Reddy,[2] M. Tarique Hussain,[2,6] Munes Fares,[2] Thomas Carroll,[5] Andrew D. Spearman,[3] and Ondine Cleaver[1]*

[1]Department of Molecular Biology, University of Texas Southwestern Medical Center, 5323 Harry Hines Blvd., Dallas, Texas, USA 75390.
[2]Department of Pediatrics, Division of Cardiology, University of Texas Southwestern Medical Center, 5323 Harry Hines Blvd., Dallas, Texas, USA 75390.
[3]Department of Pediatrics, Division of Cardiology, Medical College of Wisconsin, Children's Wisconsin, Herma Heart Institute, Milwaukee, Wisconsin, USA.
[4]Cardiovascular Center, Medical College of Wisconsin, Milwaukee, Wisconsin, USA..
[5]Department of Internal Medicine and Division of Nephrology, University of Texas Southwestern Medical Center, 5323 Harry Hines Blvd., Dallas, Texas, USA 75390.
[6]Department of Radiology, University of Texas Southwestern Medical Center, 5323 Harry Hines Blvd., Dallas, Texas, USA 75390.

*Corresponding author:
Ondine Cleaver
Department of Molecular Biology,
University of Texas Southwestern Medical Center
5323 Harry Hines Blvd., NA8.300
Dallas, Texas 75390-9148, USA.
Phone: (214) 648-1647
Fax: (214) 648-1196
E-mail: ondine.cleaver@utsouthwestern.edu

Running title: **Pulsatile stretch drives mural thickness**
Word Count: 8,456

Keywords: PDGFB, endothelial cell, mural cell, biomechanical force, hemodynamics, pulsatility, Glenn, single ventricle, congenital heart disease, rat, mouse

Non-standard Abbreviations and Acronyms

AV - arteriovenous
HAECs - human aortic endothelial cells
HPAECs - human pulmonary arterial endothelial cells
LPA - left pulmonary artery
L-SVC - left superior vena cava
NHLFs - normal human lung fibroblasts
PA - pulmonary artery
PASMCs - human pulmonary artery smooth muscle cells
PAVMs - microvascular pulmonary arteriovenous malformations
PDGFB - platelet derived growth factor B
PDGFR β - platelet derived growth receptor β
RPA - right pulmonary artery
SVC - superior vena cava
SV-CHD - Single ventricle congenital heart disease
vSMC - vascular smooth muscle cell

ABSTRACT

BACKGROUND

Single ventricle congenital heart disease (SV-CHD) is a uniformly lethal condition. Survival depends upon the Glenn surgery, which shunts venous blood directly to the pulmonary arteries without the support of a pumping ventricle. In the context of this altered circulation (loss of cardiac-driven pulsatility), diverse pulmonary vascular complications develop, severely limiting survival. To date, the relationship between loss of arterial pulsatility and pulmonary vascular changes has not yet been investigated at the cellular level.

METHODS:

Using combined cardiac catheterization and cardiac MRI, we defined pulsatility loss in three dimensions (flow, pressure, and stretch) in the pulmonary arteries of SV-CHD patients in the Glenn stage. To assess the impact of pulsatility loss on endothelial cells (ECs), we exposed cultured human pulmonary artery endothelial cells to individual dimensions of force. We used bulk RNA sequencing, GSEA, ELISA, and immunofluorescent staining to investigate cellular changes. A rat model of the Glenn circulation was used to further assess the cellular adaptation of pulmonary arteries to non-pulsatile hemodynamic forces.

RESULTS:

We identify and quantify pulsatility loss in Glenn patients, occurring in all three dimensions of hemodynamic force. We show unique transcriptional signatures of pulsatility within each dimension of force, affecting key structural and signaling pathways in ECs. We identify pulsatile stretch as a critical stimulus for endothelial secretion of PDGFB—a known driver of vascular smooth muscle cell (vSMC) proliferation and vascular wall recruitment. Moreover, we show that loss of arterial pulsatility *in vivo* leads to thinning of the vascular wall and reduction of VSMCs.

CONCLUSIONS:

This work identifies a novel and critical role for blood flow pulsatility in maintenance of the pulmonary vascular architecture. Our study provides a mechanistic understanding of the role of pulsatile, arterial forces in maintaining normal pulmonary vascular architecture through EC-SMC crosstalk. Arterial pulsatility is sensed by stretch of endothelial cells and relayed via PDGFB to the vascular smooth muscle, thus maintaining a vascular structure that can support arterial hemodynamic force.

Clinical Perspective

What is new?

- Using simultaneous cardiac MRI and cardiac catheterization, we provide the first complete, three-dimensional characterization of pulmonary arterial pulsatility loss in Glenn patients.
- Within each dimension of hemodynamic force—laminar flow, pressure, and circumferential stretch—pulsatility drives unique changes in the transcriptional profile of endothelial cells.
- Pulsatile stretch is the primary stimulant of PDGFB secretion in pulmonary endothelial cells, highlighting the importance of stretch to critical EC functions.
- Rat model of Glenn surgery shows thinning of the vSMC layer of pulmonary arteries.

What are the clinical implications?

- For a flow-focused field, this work provides a mechanistically-based rationale to assess vascular stretch in our patients with congenital heart disease.
- Efficacy of attempts to restore pulsatility in single ventricle congenital heart disease patients can now be evaluated quantitatively using combined cardiac MRI and cardiac catheterization.
- Pulsatility-sensitive signaling pathway signatures provide a toolkit for analysis and treatment of vascular complications in other clinical scenarios where pulsatility is lost (ventricular assist devices) or gained (arteriovenous fistula formation for dialysis access).

INTRODUCTION

Life with a single cardiac ventricle is a precarious proposition. A single ventricle cannot perform the work of two for very long, nor can it direct an equal amount of blood flow to the lungs (low vascular resistance) and the body (high vascular resistance). For children with single ventricle congenital heart disease, survival depends on a series of remarkable surgeries. In the circulation created by the Glenn and Fontan procedures, venous blood flows directly to the lungs without the support of a pumping ventricle, while the single functional ventricle supplies pulsatile flow to the systemic circulation.

The loss of pulsatile flow by a supporting ventricle is not without cost, as myriad complications develop—and all with unclear etiologies. Diffuse microvascular pulmonary arteriovenous malformations (PAVMs) often arise during the Glenn stage, while the progressive development of diverse, tortuous collateral vessels complicate blood flow and oxygenation in both stages.[1] Among the abundant potential pathogenic factors—chronic hypoxemia, chronic inflammation, and loss of direct hepatopulmonary blood flow[2-4]—the role of pulsatility has yet to be fully investigated.[5-7]

Pulsatility, for its part, is a critical characteristic of arterial blood flow. Arteries—whether systemic, pulmonary, or umbilical—are clinically *defined* by the presence of pulsatile blood flow, not by their color or oxygen content. However, while the magnitude of fluid shear is often considered, the role of *pulsatility* in maintaining normal arterial or venous endothelial cell (EC) function has received very limited attention.[8,9]

ECs are remarkably sensitive to force. Their mechanosensitive signaling components include cell-cell adhesion molecules (integrins, gap-junctions, cadherins), extracellular matrix sensing components, ion channels, and more.[10,11] The forces sensed by these molecular components are applied to ECs in three dimensions: laminar flow, pressure, and stretch.[12] Each dimension of force is reasonably expected to exert different stresses and deformations to ECs—likely driving different transcriptional programs in response to these unique stimuli. Stretch in the circumferential axis can be expected to repeatedly deform the EC, possibly driving structural reinforcement of cellular and extracellular matrix (ECM) components. Hydrostatic pressure, as the driving force behind stretch, might well activate similar transcriptional programs. Alternatively, for a single endothelial cell, pulsatility of flow might not detectable after alignment to flow has been achieved. The impact of pulsatility of hemodynamic force on vascular homeostasis thus remains a critical knowledge gap.

Recent work has identified critical differences between arterial and venous ECs, often pertaining to proliferative state and migratory direction.[13,14] While this work is critical for understanding the endothelium in vasculogenesis, the vascular structure as a whole—intima, media, and adventitia—is formed to serve the unique function of artery and vein, and to withstand the unique hemodynamic forces they experience over a lifetime. Large arteries depend upon the presence of an internal elastic lamina and a thick layer of the smooth muscle, while veins require less structural support. Critically, cross-talk between EC and vascular smooth muscle cells (vSMCs) is mediated by EC-secretion of platelet derived growth factor B (PDGFB), which binds to PDGF receptor β (PDGFR β) on VSMCs, where it drives proliferation and dictates mural cell coverage from large vessels down to the capillary level.[15,16] Recent work deleting PDGFB specifically from ECs has shown remarkable dilation and arteriovenous shunting in the lungs of mice,[17] and loss of PDGFB has been observed in human vascular malformations.[18]

While shear stress does induce PDGFB secretion from ECs, the flow-responsive secretion of PDGFB decreases both with time and with higher shear stress.[19] Pulsatile stretch, however, has been reported to induce EC PDGFB production more stably at 4 hours of stretch.[20] As ECs are in direct contact with all three dimensions of hemodynamic force, they are uniquely positioned to coordinate the maintenance of vascular structure in response to pulsatility of force. We seek to understand the unique or complementary roles of hemodynamic force in three dimensions as it relates to the pulmonary vascular changes seen in the Glenn circulation.

In this work, we investigate the biomechanical forces experienced by pulmonary ECs in Glenn patients and identify pulsatility of blood flow as critical to maintenance of the lung vasculature. We first use combined cardiac catheterization and cardiac magnetic resonance imaging (MRI) to quantify and compare the pulsatility of force that is applied to ECs in children with normal cardiopulmonary anatomy and in those with Glenn circulation. After noting a clear loss of pulsatility in the Glenn pulmonary arteries, we model those changes using cultured human pulmonary arterial endothelial cells (HPAECs) to define the specific transcriptional programs driven by each individual dimension of force. We demonstrate that pulsatile flow *in vitro* stimulates ECs to secrete PDGFB. Finally, using an *in vivo* rat model of the Glenn surgery, we demonstrate that loss of arterial pulsatility results in thinning of the arterial vascular walls. In this study, we identify pulsatile stretch as the critical dimension of arterial force that drives EC-secretion of PDGFB to promote vascular smooth muscle growth, thereby providing structural support for arterial vessels. Gaining insight into the impact of *pulsatility* of hemodynamic force is a critical and novel approach to understanding of clinically relevant endothelial cell biology.

MATERIALS AND METHODS

Data Availability

All sequencing data that support the findings of this study have been deposited in the National Center for Biotechnology Information Gene Expression Omnibus (GEO) and are accessible through the GEO Series accession number GSE298790. All other relevant data are available from the corresponding author on request.

Combined cardiac catheterization and cardiac MRI

Combined cardiac catheterization and MRI was performed on a Philips XMR setup (Phillips Ingenia Evolution, Best, Netherlands).[21] This consists of a 1.5T MRI-scanner and a BV Pulsera or Allura Clarity or Ingenia (Philips) cardiac X-Ray unit. An appropriate size balloon wedge catheter (Arrow Intl., Reading, PA) and receiver coil were used depending on the weight of the patient.

All studies were conducted under general anesthesia based on clinical need. Patients were recruited and data was recorded in sequence of the patient's referral for the procedure under University of Texas Southwestern IRB-approved study (STU 032016-009) in 2023 - 2024. All Glenn patients with a single functional ventricle were considered for inclusion in the study. Patients were excluded if they had pulmonary blood flow in addition to the flow provided by the Glenn anastomosis.

227 Pulsatility was assessed by pulse difference, which was defined as the difference between
228 maximum and minimum value for each parameter of force. For each 2D cross-section of
229 the right pulmonary artery obtained, we obtained a mean velocity (averaged over the cross
230 section of the vessel). This data is obtained over 1 to 2 minutes 'free-breathing' using
231 phase contrast velocity-encoded cine MRI. Sequence parameters included 40 cardiac
232 phases, TE/TR = 2.7/4.4 ms (TE = echo time, TR = repetition time), with two signal
233 averages, 1.5-2mm × 1.5-2mm × 6-8 mm resolution, SENSE acceleration factor = 2, with
234 the velocity encoding gradient set to 25% above the expected maximum velocity in each
235 vessel. Vendor-provided background phase correction was used. Artificial intelligence-
236 assisted segmentation using Circle (Circle Cardiovascular Imaging, CVI42, v6.1.2) was
237 performed to obtain the maximum and minimum area, from which an idealized
238 circumference was calculated. Pressure tracings were obtained on a standard Siemens
239 Sensis Hemodynamic recording system (Siemens Healthineers, Munich, Germany), using
240 a 5- or 6-French Arrow, Balloon Wedge-Pressure Catheter (Teleflex Medical Headquarter
241 International, Ireland) located in the proximal right branch pulmonary artery.
242
243 ***In vitro* cell based assays of pulsatile force**
244 Pulsatile force was applied to confluent monolayers of human pulmonary artery endothelial
245 cells (HPAECs, Lonza) for 48 hours under each condition. Pulsatile (1 Hz, 15 dyn/cm^2) and
246 continuous (15 dyn/cm2) shear was applied using the Ibidi system (Ibidi USA, Wisconsin).
247 Pulsatile (25-5 mm Hg) and continuous (25 mm Hg) pressure was applied using a custom
248 modification to the Ibidi system whereby cells were alternately (1 Hz) exposed to columns
249 of culture media to deliver the desired hydrostatic pressure. Pressure readings were tested
250 and confirmed the using the Siemens Sensis Hemodynamic recording system listed
251 above. Pulsatile stretch was applied using Uniflex plates (1Hz, 1 hr of 3% stretch for
252 acclimation followed by 47 hrs of 10% stretch) as a part of the Flexcell FX-6000 system
253 (Flexcell International, Burlington, NC). Ibidi channels were pre-coated with the proprietary
254 Ibi-treat to promote cell adhesion, and Flexcell uniflex plates were coated with 0.1% gelatin
255 to promote cell adhesion.
256
257 All experiments utilized at least three biological replicates, using separate aliquots of
258 HPAECs from two different donors. RNA was extracted using RNeasy Plus kit (Qiagen)
259 prior to bulk RNA sequencing. Library generation and bulk RNA sequencing was carried
260 out by the McDermott Next Generation Sequencing core facility at UT Southwestern
261 Medical Center, using an Illumina NextSeq 2000. Processed sequencing data (using
262 iGenomes annotations) was provided by the core, and a TPM cutoff of 10 was applied (if
263 any test condition resulted in a gene's TPM >10, the gene was included in our analysis).
264
265 For pathway analysis, we performed gene set enrichment analysis was performed for sets
266 curated in MsigDb (PMID 26771021) using with fgsea (BioRxiv
267 https://doi.org/10.1101/060012) Bioconductor package. To simultaneously account for both
268 the magnitude and significance of the measured effects, genes were ranked by the
269 quotient of log fold-change and adjusted P-value.
270
271 **Human Lung Single Cell RNA sequencing**
272 The LungMAP Human Lung CellRef atlas was utilized via the online portal at
273 www.lungmap.net. [22,23] This dataset includes 148 normal human lung samples from 104
274 donors, including child, adolescent, and adult tissue. Tissue types include parenchyma,

trachea, bronchi, bronchus, and small airways. 347,970 cells from the dataset were included in our analysis. Both ShinyCell and cell x gene were utilized for visualization of cell-specific gene expression. Dataset ID: LMEX0000004396.

Measurement of PDGFB secretion *in vitro*

Cultured HPAECs, human arterial endothelial cells (HAECs, Lonza), human pulmonary artery smooth muscle cells (PASMCs, Lonza), and normal human lung fibroblasts (NHLFs, Lonza were plated onto Flexcell uniflex plates (pre-coated with collagen I). Each cell line was grown in the recommended cell culture media, obtained from Lonza: HPAECs and HAECs were grown in EGM-2, PASMCs in SmGM-2, and NHLFs in FGM-2. Cells were grown to confluency then subjected to pulsatile stretch for 48 hours as above. Media was collected and PDGF-BB was measured by ELISA (R+D systems DY220). For comparison to endothelial cells under flow, media was obtained from confluent HPAECs in 6 well plates under continuous flow at 15 dyn/cm^2 shear stress in a rotational flow apparatus (Thermo Scientific Model No: 88881101).

For measurement of transpulmonary gradient of PDGF-BB (here termed PDGFB) in human plasma, samples were obtained directly from Glenn and heart transplant patients in the course of regularly indicated cardiac catheterization. Patients were consented for the IRB approved study (University of Texas Southwestern IRB: UTSW-2020-0047). Samples were obtained from the pre-capillary blood (right pulmonary artery) and the post-capillary blood (right pulmonary wedge position, with the catheter in the distal pulmonary artery with balloon inflated and the sample drawn through the end hole) in each patient. Nature of each sample as pre- or post-capillary was then confirmed by prompt measurement of oxygen saturation, and only fully oxygenated samples were used for the analysis. All samples were obtained in K2-EDTA purple-top tubes, placed on ice, and promptly spun down for plasma isolation. Samples were stored at -80°C up to 2 years maximum prior to measurement by ELISA as above.

Surgical Rat Model of Glenn Circulation

The rat surgical model of Glenn circulation is described in detail previously.[24] Briefly, we performed an end-to-end cavopulmonary anastomosis between the left superior vena cava (L-SVC) and the left pulmonary artery (LPA). This was previously shown to result in progressive impairment (beginning by two weeks) in oxygenation in tandem with the development of intrapulmonary arteriovenous shunts as detected by both bubble echocardiography and microsphere injection.

Adult Sprague–Dawley rats (male and female, 6–12 weeks of age) were used for all experiments (Taconic). All rats were housed in the Biomedical Research Center at the Medical College of Wisconsin with access to standard chow diet (PicoLab Lab Diet, 5L0D), water ad libitum, and maintained in a 12-hour light/dark cycle. All surgical procedures were performed under isoflurane anesthesia (1%–3%). All experimental protocols were approved by the Medical College of Wisconsin Institutional Animal Care and Use Committee prior to initiation of experimental protocols (Animal Use Agreement #7731).

Tissue Preparation and Immunohistochemistry

Lungs were harvested at 2 and 6 months after surgery for these experiments. Lungs were inflated to 10 mmHg for 10 minutes with 10% neutral buffered formalin to promote normal

alveolar architecture in sections, followed by overnight fixation in 10% neutral buffered formalin. Formalin-fixed, paraffin-embedded sections were prepared using the left lung of the Glenn and sham operated animals. IHC staining was done for SMA (Abcam, ab7817) using the Leica Bond Rx automated staining platform with Leica BOND Polymer Refine Detection kit (Leica, DS9800) per manufacturer instructions, using standard labeled-streptavidin-biotin detection with secondary antibody (Jackson Immuno Research Labs, Biotinylated donkey anti-mouse 1:500, #715-066-151), streptavidin HRP (Vector Laboratories, #SA-5004), and DAB chromogen (BioCare, BDB2004). Slides were scanned using Hamamatsu HT whole slide scanner (Hamamatsu, USA) and analyzed with QuPath (Edinburgh, V0.5.1). The file names were randomized and blinded prior to analysis. Due to the possibility of changes in vessel size between sham and Glenn-operated rates, measurements were taken from the most proximal pulmonary arteries and veins to ensure a valid comparison between samples. Arteries were differentiated from veins in consultation with a trained pathologist, by their classic histological characteristics and anatomical proximity to the mainstem bronchi. Slides were not utilized for measurement if no major bronchi or large vessels could be identified. Measurements were taken only in areas where the thickness was uniform and the endothelial cells formed a clear monolayer, to avoid artifactual error from the angle of the slice.10 measurements of each large vessel (artery or vein, Glenn or sham-operated) were obtained, and the mean measurement value was used for analysis.

Statistical Analysis

Sample sizes were based on patient availability and standards in the field. Data were both analyzed and plotted in Graphpad PRISM 10.2.3. Descriptive statistics (mean, standard deviation, median, min, and max) were employed for summarizing demographic, hemodynamic, and clinical variables. Statistical tests (indicated in the relevant methods sections and figure legends) utilized were the parametric unpaired Student's *t*-test and the 2-Way ANOVA with Tukey's multiple comparisons test. Statistical significance is noted as follows: ns = $p > 0.05$; * = $0.01 < p < 0.05$; ** = $0.001 < p < 0.01$; *** = $0.0001 < p < 0.001$; **** = $p < 0.0001$. Cell images were analyzed in FIJI. Figures and models were made using Microsoft PowerPoint, data were partially analyzed in Microsoft Excel, and text was written in Microsoft Word.

RESULTS

The Glenn shunt directs venous blood flow to arteries

Arterial vessels normally experience blood flow directly from a pumping ventricle that lends pulsatility to the magnitude of forces (**Figure 1a**). By reviewing the known characteristics of three distinct pairings of arteries and veins (systemic, pulmonary, and umbilical), we note that pulsatile flow is a shared, definitional quality of arteries (**Supplemental Figure 1**). Pulsatility is thus an inherent quality of blood flow in arterial vessels. After a Glenn surgery, however, the pulmonary arteries no longer receive blood flow directly from a pumping ventricle. Instead, pulmonary blood flow is provided by the Glenn shunt: direct venous flow through the superior vena cava, which is anastomosed to the pulmonary arteries (**Figure 1a'**).

Pulsatility loss in three dimensions in Glenn patients

To quantitatively determine the loss of pulmonary arterial pulsatility in patients with Glenn anatomy, we used combined cardiac catheterization and cardiac MRI in 20 Glenn patients to obtain simultaneous data in all three dimensions of force: pressure, flow, and circumferential stretch (**Figure 1b**). These data were compared to data obtained in 20 age- and gender-matched patients with normal cardiopulmonary connections (see patient demographics in **Supplemental Table 1**). First, as has long been observed clinically, we observed pulsatility loss in the pulmonary artery pressure of Glenn patients (**Figure 1c, c'**). Similarly, we noted that the Glenn shunt leads to non-pulsatile blood flow in the pulmonary arteries, displayed by a comparison of the pulmonary artery velocity profiles in normal (**Figure 1d**) and Glenn (**Figure 1d'**) patients throughout the cardiac cycle. Finally, we found that the circumference of proximal right pulmonary artery does not change appreciably with the cardiac cycle in Glenn patients, demonstrating loss of circumferential stretch (**Figure 1e, e'**).

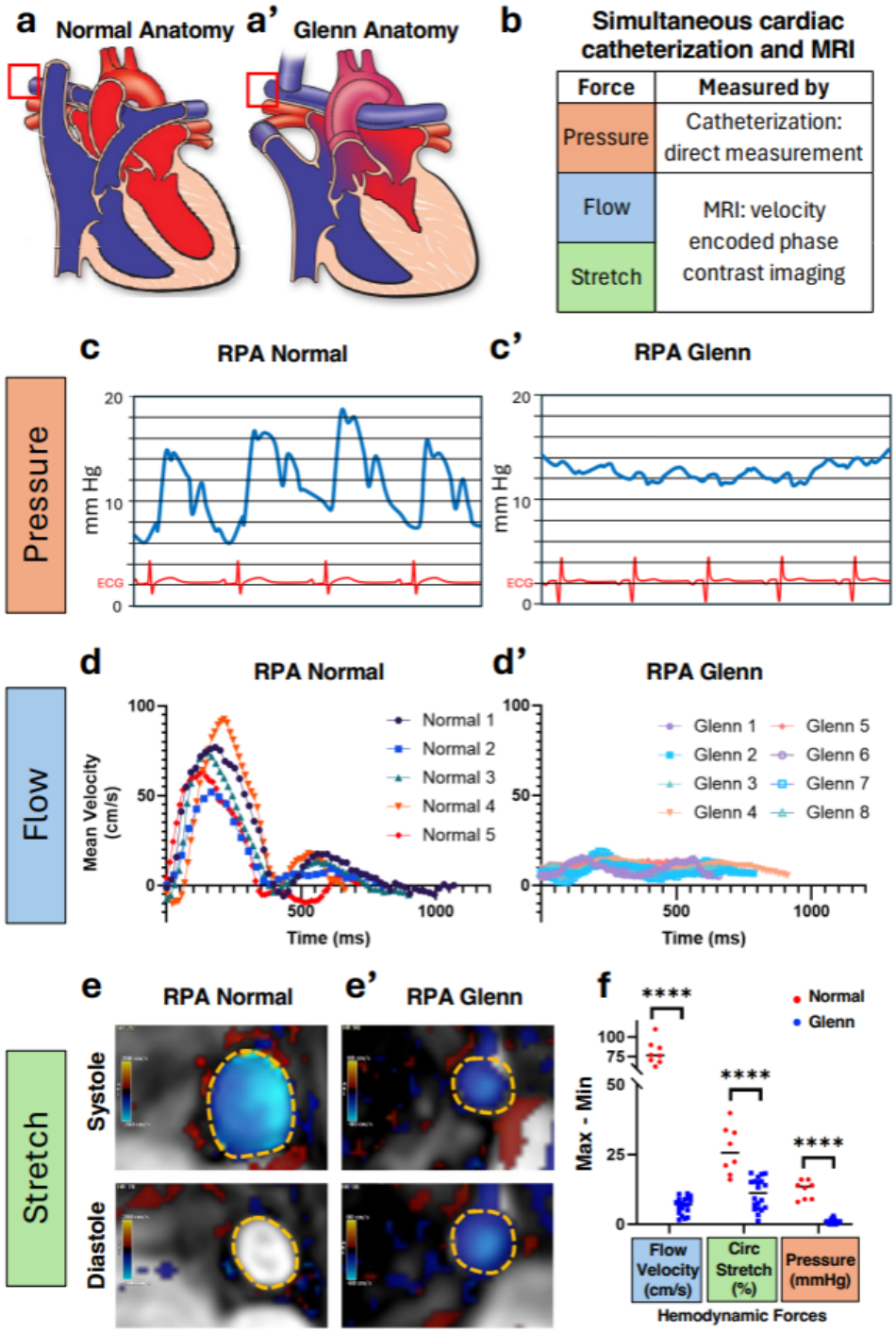

Figure 1: Loss of pulsatility in three dimensions within Glenn pulmonary arteries. a, a' Diagrams of representative normal and Glenn cardiopulmonary anatomy. Red boxes highlight location of force pulsatility measurements. **b** Outline of data collection method for each dimension of hemodynamic force. **c, c'** Example pressure waveforms from the right pulmonary artery of normal and Glenn patients. Electrocardiogram shown in red for correlation to cardiac cycle. RPA, right pulmonary artery. **d, d'** Variation in flow velocity of the proximal right pulmonary

artery measured by cardiac MRI throughout a cardiac cycle from systole (start) to end-diastole (end). Variability in length of time for each patient reflects the variable heart rate within each subject. **e, e'** Cardiac MRI velocity encoded phase contrast images with color showing velocity of blood flow out of the plane of the image slice. Dotted orange line shows RPA border. RPA diameter increases during systole in anormal patients, but does not increase during systole in Glenn patient. **f** Quantification of pulse difference of each dimension of force, obtained during combined cardiac catheterization and cardiac MRI of normal (n=20) and Glenn (n=20) patients, demonstrating loss of pulsatility in the Glenn. Circumference % change is calculated from baseline in diastole.

Unique transcriptome for each dimension of pulsatile force

The ECs that make up the inner lining of blood vessels are exposed to force in three dimensions: flow/shear stress, pressure, and circumferential stretch (**Figure 2a**).[12] ECs are highly responsive to mechanical force, and can react to differences in both magnitude and direction of force.[26] Given the observed loss of pulsatility in Glenn patients, we next investigated the relative impact of pulsatility within each dimension of force on ECs.

To begin, we used our patient cath/MRI pulsatility data to design *in vitro* experiments modeling the pulsatility loss defined in Glenn patients. Each isolated, single dimension of force was applied to cultured primary human pulmonary artery endothelial cells (HPAECs) in a pulsatile and non-pulsatile manner. For pulsatile laminar flow, we applied 0-15 dyn/cm^2 shear stress at 1 Hz. For pulsatile pressure, we modified the Ibidi equipment to expose HPAECs to columns of media positioned to alternate providing 5 or 25 mmHg pressure, at 1 Hz, in the absence of flow or stretch. For stretch, we used the Flexcell system to stretch HPAEC by 10% of their baseline in a single axis (again at a frequency of 1 Hz). To assess stable transcriptional changes between non-pulsatile and pulsatile conditions and thus improve *in vivo* relevance of our findings, HPAECs were exposed to 48 hours of force or pulsatile force (**Figure 2b**).

We first investigated the overall pathways that were regulated by pulsatility. By gene set enrichment analysis of bulk RNAseq data, we noted that each dimension of force drove changes in unique signaling pathways, and that the impact of flow was the most distinct. Overall, in HPAECs, laminar flow affected 19 unique pathways, stretch 10 unique pathways, and pressure 4 unique pathways (**Figure 2c**). The expected cell shape adjustments to force (ECs align in the direction of flow and perpendicular to the direction of stretch) were observed (**Figure 2d**). A wide range of pathway types were regulated, many related to changes in structural cellular components, growth, or interaction of the cell with ECM (**Figure 2e**). We note that mitogen-activated protein kinase (*Mapk*) and epidermal growth factor receptor (*ErbB*, also known as *HER*) signaling were only induced by pulsatility of flow, while Hedgehog and Notch signaling were only induced by pulsatility of stretch. Pulsatility pressure did not regulate any obvious EC-related pathways, but did upregulate the hypertrophic cardiomyopathy pathway.

In addition to these dimension-specific pathways, we find other pathways that are influenced across multiple dimensions of force. We found 10 pathways upregulated by all 3 dimensions of force, and 17 pathways induced by two of the three dimensions. We note that flow, stretch, and pressure all drove changes in the pathway "Regulation of Actin Cytoskeleton." However, an analysis of the leading-edge subset (the genes within the pathway that are most significantly changed and thus responsible for the overall significance of the pathway) revealed upregulation of different genes by each dimension of

force. For example, within the “Regulation of Actin Cytoskeleton” pathway, pulsatile stretch promotes *Itgb5, Pdgfb*, and others, while pulsatile pressure shows *Actn1* and pulsatile flow yields *Raf1*, among others (data not shown). Different dimensions of force drive different transcriptional changes that converge on similar pathways.

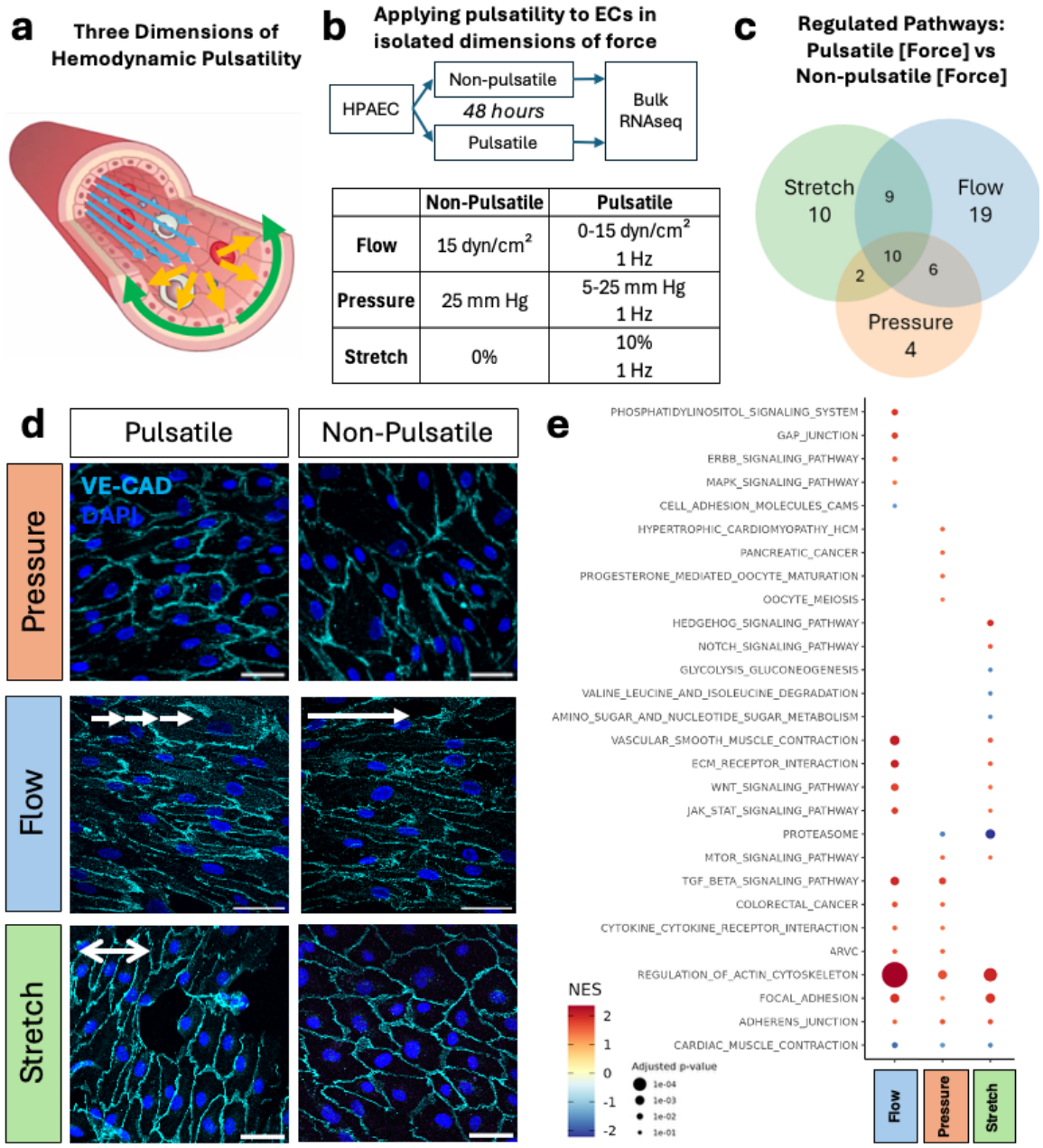

Figure 2: Pulsatility drives distinct signaling pathways within each dimension of force. a Hemodynamic forces act on ECs in three dimensions: shear/flow (blue), pressure (orange), and circumferential stretch (green) **b** Experimental conditions: HPAECs were exposed to 48 hours of a single dimension of either non-pulsatile or pulsatile force, and bulk RNA sequencing was performed. **c** GSEA of bulk RNAseq data shows overlapping and unique pathways activated by each dimension of force.

d Representative images of the cell-shape adjustments that occur in response to the different forces are shown. **e** Normalized enrichment score (NES) and adjusted p-value (adj p-val) shown for select signaling pathways shows greater impact of pulsatility within flow and stretch relative to pulsatility of pressure.

Pulsatility does not alter arteriovenous genes *in vitro*

We next analyzed the expression of individual genes, which affirmed that each dimension of force has a unique transcriptional signature. Utilizing again the bulk RNAseq data obtained after application of single dimensions of pulsatile and no-pulsatile force (using the devices shown in **Figure 3a**), we found very little overlap between different dimensions. We did not find significant changes in baseline expression of common EC genes between the three experimental set-ups (**Supplemental Figure 2**). Of the genes significantly regulated by pulsatility, 93.4% (1205/1290) were driven by a single, unique dimension of force. Pulsatility of stretch accounted for over two-thirds (888 genes, 68.9%) of these genes (**Figure 3b**). Only 59 genes were uniquely induced by pulsatility of laminar flow, while 343 were uniquely induced by pulsatility of pressure.

There was less overlap in individual genes regulated by pulsatility than there was in overall pathways. We found that 22 genes were regulated by pulsatility of both flow and stretch, 56 genes by stretch and pressure, and 5 by pressure and flow. Only 1 gene (*Fam84b,* also known as *Lratd2*) was significantly induced by pulsatility within all three dimensions of force (**Figure 3b**).

Finally, we hypothesized that pulsatile force would induce greater expression of genes previously shown to be specific to arterial ECs.[27] We asked whether the classical markers of arteriovenous (AV) differentiation were found in these groups of genes. In cultured HPAECs, we found no dimension of pulsatility that significantly affected the expression of developmental arterial (*Efnb2*, *Sox17*, *Notch1*) or venous (*Ephb4*, *Emcn*, *Coup-TFII*) driver genes (**Figure 3c**). After applying a p-value cut-off of 0.05 and fold change cut-off of 2, we found that stretch drove a change in 44 genes, compared to 20 genes by pulsatility of flow, and 16 genes by pulsatility of pressure (**Figure 3d-f**). Expression of these hits in data from other dimensions of force is shown in **Supplemental Figure 3**. We did not find any other genes that have been reported to specifically mark ECs within arteries or veins.

Identification of *PDGFB* as a stretch-induced gene

As stretch accounted for the majority of pulsatility-regulated genes, we utilized published single cell RNA sequencing of human lung tissue (LungMAP[22,23]) to assess the cell type-specific expression pattern of candidate genes. *Mgp*, *Cx3cl1*, and *Pdgfb* were highly expressed in a good proportion of ECs under stretch, but we noted high EC specificity of the latter two genes (**Figure 4a**). Analysis of the expression of these ligands and their receptors (*Cx3cl1R* and *Pdgfb*, respectively) underscored the pulsatility-induced crosstalk between ECs and immune cells (for *Cx3cl1*) and between ECs and perivascular cells (for *Pdgfb*) (**Figure 4b-d**). As PDGFB is a) well known to promote smooth muscle cell proliferation and recruitment,[15] b) a key component of the gene set enrichment analysis for ECs under stretch (**Figure 2**), and c) a significant hit in their differential gene expression (**Figure 3**), PDGFB thus presented itself as worthy of further investigation.

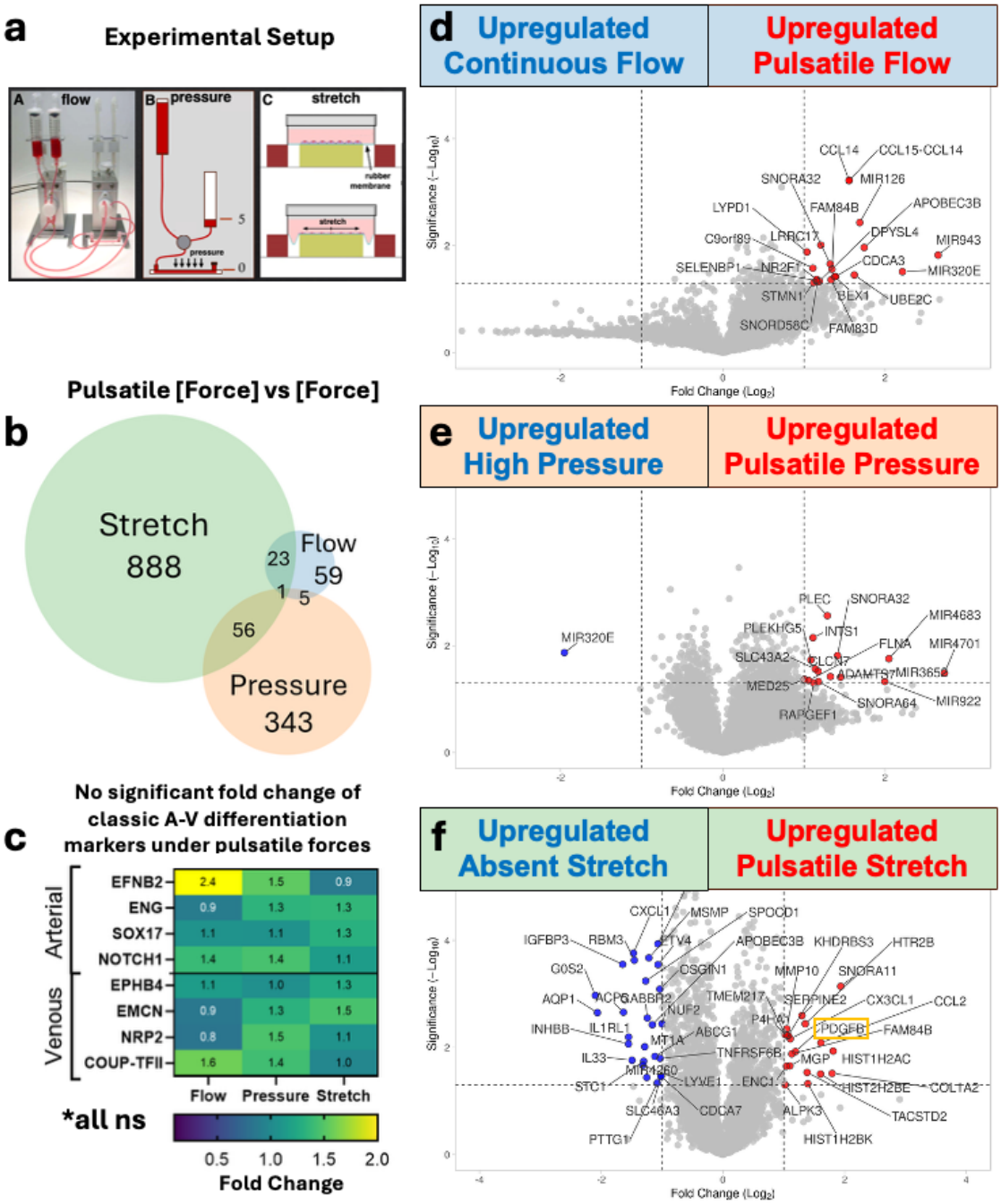

Figure 3: Impact of pulsatile stretch is greater than pulsatile pressure or flow, but does not change classical arteriovenous differentiation. a Diagram of cell culture setup to apply isolated dimensions of force to ECs. **b** Venn diagram of the number of genes significantly up- or down-regulated by pulsatility of flow, pressure, or stretch. **c** Fold change (pulsatile/non-pulsatile) of any classic EC arteriovenous differentiation markers by bulk RNAseq. Color scale denotes fold change, exact number in each box. All values were not significant (ns), with p-values > 0.05. **d, e, f** Volcano plots of significantly regulated genes within each dimension of pulsatile force.

510
511 **Pulsatile stretch uniquely drives EC PDGFB secretion**
512 We next asked if stretch-induction of PDGFB induction was specific to ECs or also
513 present in other cellular components of the vessel wall (vascular smooth muscle or
514 fibroblasts). We applied 10% stretch to HPAECs from two different patients, human aortic
515 endothelial cells (HAECs), human pulmonary artery smooth muscle cells (PASMCs), and
516 normal human lung fibroblasts (NHLFs). Pulsatile stretch robustly induced secretion of
517 PDGFB exclusively from endothelial cell lines (**Figure 4e**). As PDGFB is known to be
518 induced by flow,[28] we compared PDGFB secretion from ECs under continuous flow
519 (venous condition) to pulsatile stretch (arterial condition). Induction of PDGFB by pulsatile
520 stretch was 5x higher than the induction by laminar, continuous flow (**Figure 4f**).
521 We next assessed whether ECs in human patients might display similar pulsatile
522 stretch-induced secretion of PDGFB. To do this, we assessed whether loss of pulsatile
523 stretch in the pulmonary arteries of Glenn patients was associated with loss of PDGFB
524 downstream, in the pulmonary venous blood. We anticipated that there would be little to no
525 effect, as PDGFB would likely be secreted basally to the perivascular space, not apically
526 into the blood stream. Analysis of PDGFB expression in plasma obtained from the
527 pulmonary artery and pulmonary vein revealed significant variation in local PDGFB
528 expression in both normal and Glenn patients that could not be correlated with pulmonary
529 arterial pulsatility (**Figure 4g**).
530
531 **Rat Glenn displays reduced pulmonary arterial smooth muscle**
532 Given the finding that stretch induces PDGFB secretion from pulmonary endothelial
533 cells, we utilized our animal model of the Glenn surgery to replicate *in vivo* the loss of
534 pulsatility and stretch that is seen in patients with the Glenn circulation. As previously
535 published, we performed a rat classic Glenn surgery—specifically, a direct end-to-end
536 anastomosis of the left superior vena cava to the left pulmonary artery.[24] These rats
537 develop hypoxemia secondary to intrapulmonary arteriovenous shunting. The hypoxemia
538 develops rapidly (after two weeks) and is progressive (to six months). We hypothesized
539 that loss of stretch would result in reduced EC secretion of PDGFB, and as a
540 consequence, we would observe a thinner smooth muscle layer. We analyzed coronal
541 sections of the left lung of 9 Glenn rats and 5 sham-operated rats and performed
542 immunohistochemistry for smooth muscle actin (SMA). Strikingly, we found a significant
543 decrease in arterial smooth muscle thickness (SMA+ cells), while venous smooth muscle
544 thickness remained unchanged (**Figure 5a-d**).
545

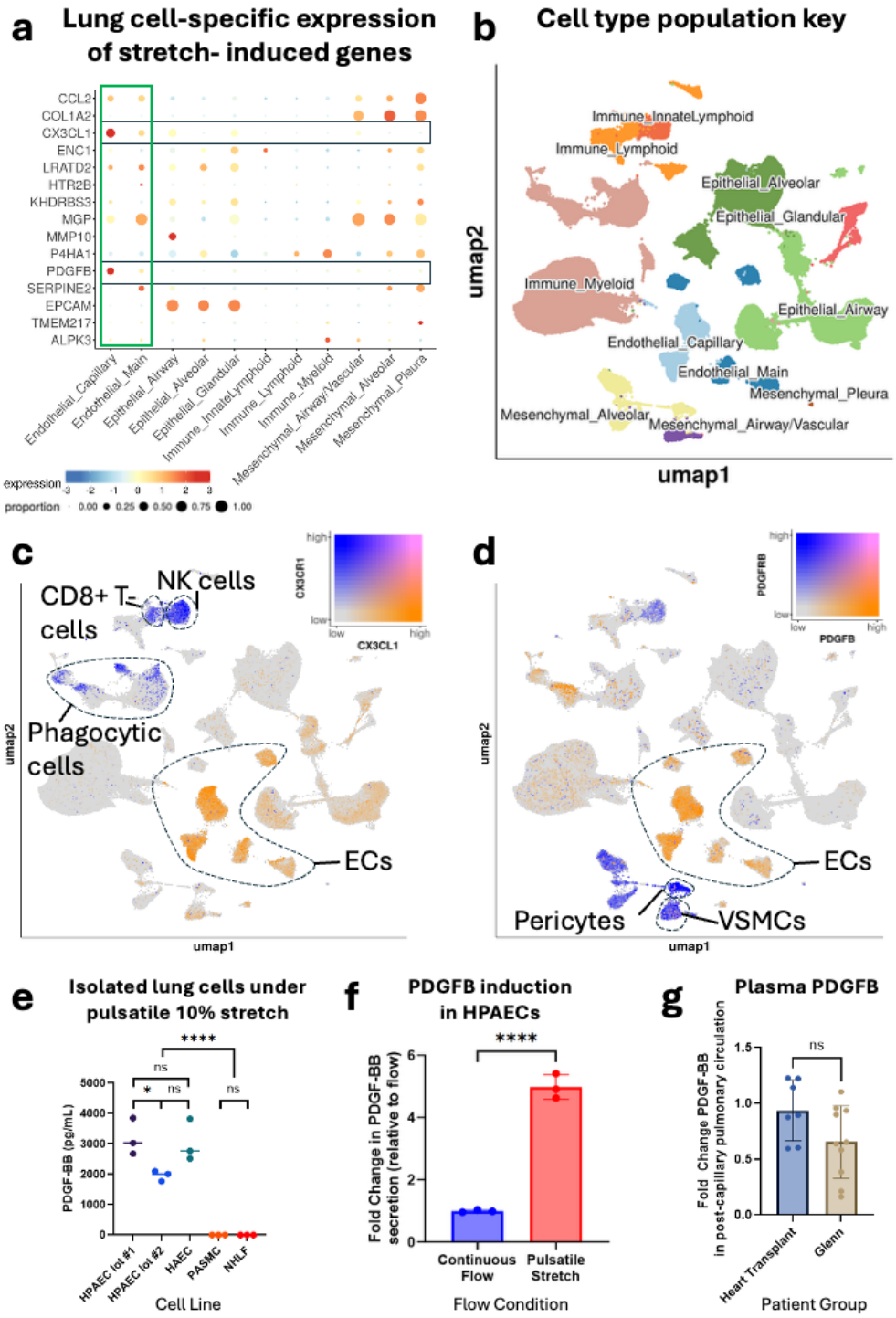

Figure 4: PDGFB expression in human lungs is endothelial-specific and stretch-induced. a Genes upregulated by pulsatile stretch in ECs were analyzed within the LungMAP single cell RNA sequencing data of human lung tissue (347,970 cells). Expression within ECs (green box) was compared to other cell types. CX3CL1 and PDGFB (black boxes) were uniquely expressed by ECs. **b** cell population groupings as annotated by LungMAP cell x gene portal. **c** Gene co-expression analysis shows expression of CX3CL1 in ECs with its receptor CX3CL1R in immune

cells. **d** Expression of PDGFB is high in ECs, with its receptor PDGFRB found in pericytes and vascular smooth muscle. **e** Different cell lines comprising the primary components of a blood vessel (endothelium, smooth muscle, fibroblasts) were exposed to pulsatile uniaxial 10% stretch at 1 Hz and only endothelial cells secreted PDGFB into the media (as measured by ELISA). **f** Pulsatile stretch of cultured HPAECs induces 5x more PDGFB secretion than continuous flow. Error bar shows 1 s.d. **g** PDGFB measured by ELISA from patient plasma does not show a significant arteriovenous concentration gradient or difference between normal and Glenn patients. Error bar shows 1 s.d.

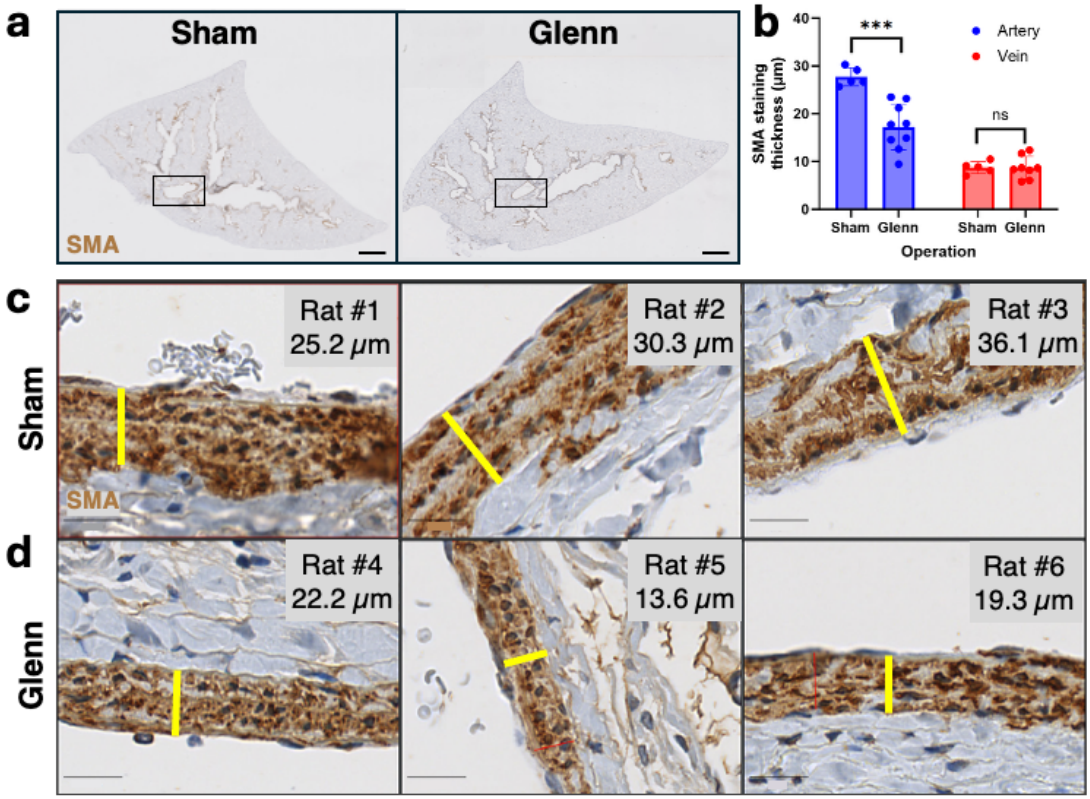

Figure 5: Loss of smooth muscle layer in pulmonary arteries of rats after Glenn surgery. a Example coronal sections of lung tissue from sham and Glenn operated rats, stained by immunohistochemistry for smooth muscle actin (SMA). Black boxes show typical perihilar location of analysis of the most proximal portions of the pulmonary artery. Scale bar = 2 mm. **b** Quantification of SMA+ media thickness in sham and Glenn operated rats at 6 months after surgery shows loss of media thickness in the Glenn, with no change of media thickness in the vein. Error bar shows 1 s.d. **c** Example images of SMA+ media thickness from 3 different Glenn rats. Scale bar = 20 μm. **d** Example images of SMA+ media thickness from 3 different sham operated rats. Scale bar = 20 μm.

DISCUSSION

In this study, we examine the impact of arterial pulsatility on the architecture of the pulmonary vasculature. We show that in patients with Glenn circulation the shunted pulmonary blood flow—from the superior vena cava (SVC) directly to the pulmonary artery (PA)—exerts no pulsatile stretch on the pulmonary artery (**Figure 6a**). Using cultured pulmonary arterial ECs, we show that each dimension of force elicits distinct molecular responses. Transcriptomic analysis of ECs exposed to pulsatile or non-pulsatile laminar shear stress, hydrostatic pressure and stretch identify distinct transcriptional signatures. We find that pulsatile stretch induces significant endothelial secretion of PDGFB, known to mediate recruitment of vSMCs to blood vessels. Using a rat model of the Glenn circulation, we demonstrate that non-pulsatile, venous flow within an arterial vessel results in thinning of the vascular mural wall and diminished vSMC coverage (**Figure 6b**). These complementary *in vitro* and *in vivo* findings identify a new target signaling pathway for novel therapeutic approaches to assuage the diverse vascular malformations that occur in Glenn patients.

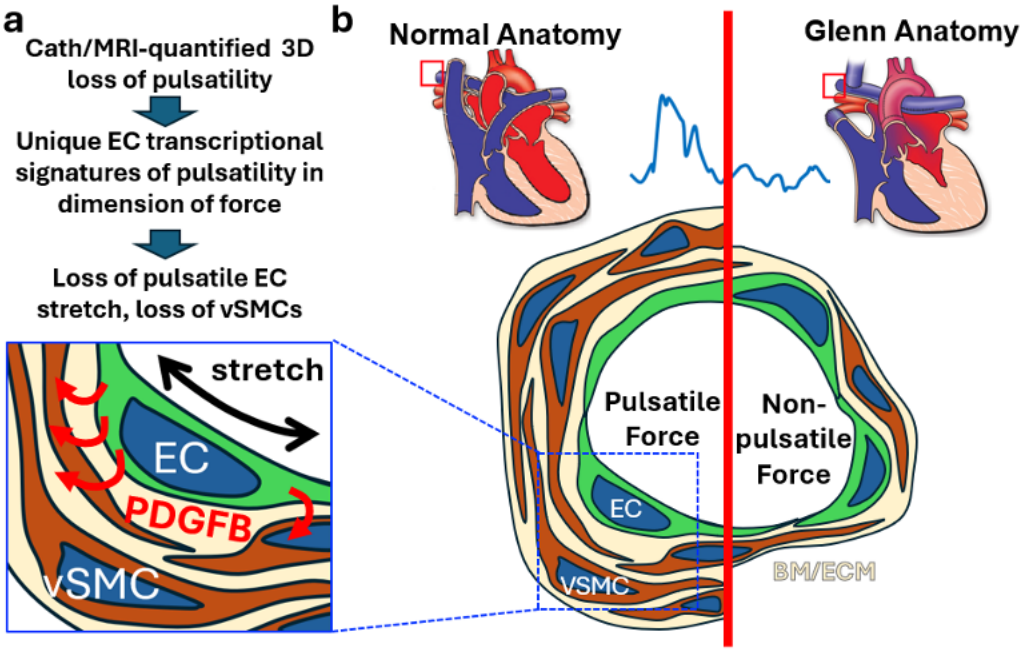

Figure 6: Summary. Outline of primary findings. **a** overview of experimental results. **b** comparison of findings between pulsatile and non-pulsatile conditions. EC, endothelial cell; vSMC, vascular smooth muscle cell; BM, basement membrane; ECM; extracellular matrix.

Despite clinical appreciation of the fact that venous blood flow is applied to the pulmonary circulation of Glenn patients, it has never been formally documented in three dimensions. Our use of combined cardiac catheterization and cardiac MRI ensures that these interdependent forces are measured simultaneously, providing a complete 3D view of pulsatility loss in the Glenn pulmonary arteries with high temporal accuracy. Studies

comparing surgical outcomes of Glenn patients have not been able to report some[5,29] or all[30-36] dimensions of pulsatility loss, limiting our understanding of the clinical impact of pulsatility within these patients. We hope that our work provides both a means and a rationale to investigate pulsatility further as we seek to understand the clinical outcomes of these highly variable patients.

We observe that the Glenn shunt supplies venous hemodynamic forces to an artery, and the artery responds by becoming structurally more like a vein. Currently, while descriptions of dilated distal vessels in the Glenn population exist, there has been no analysis of the proximal pulmonary arteries.[37,38] One publication in Fontan patients, however, has shown thinning of the pulmonary arterial media.[39] Our hemodynamic and immunohistochemical description is limited to the proximal pulmonary arteries, where measurements of pulsatility are highly reproducible in our hands and vessel branch generation is easier to determine in 2D sections. Our animal model is necessary to understand the effect of pulsatility loss, as patient biopsies cannot be easily obtained.

In a compliant vessel, proximal stretch acts as a capacitor, absorbing and lessening distal pulsatility—a phenomenon termed the 'windkessel effect'.[40] Our proposed model that pulsatile stretch of ECs stimulates smooth muscle coverage is supported by our observation that arterial smooth muscle diminishes as vessels branch further into the lung.[41] Dynamic measurement of distal pulsatility is technically challenging, regardless of modality, and has not yet been fully characterized. Further investigation of distal pulsatility (in 3D) and its relation to smooth muscle/pericyte coverage will be necessary to elucidate the effects of pulsatility throughout the lung.

Enhancement of arterial EC markers by pulsatility of shear stress has been observed previously *in vitro*.[8] We noted that the classic markers of arterial EC identity were not enhanced under pulsatile conditions in our dataset, in any dimension of force. It is possible—if unlikely—that this difference is a reflection of the highly laminar flow provided by the Ibidi system, compared to the more turbulent flow in the cone-disc viscometer used in the prior study. Separately, it was observed that microvessels exposed to arterial anastomosis have been observed to increase vSMC coverage.[42] As such, rather than the developmentally defined transcriptional arteriovenous EC identity, our work focuses on the structure of the vessel as a whole, and how different cell populations communicate: ECs sensing pulsatility and communicating (via PDGFB) their requirement for support to the mural cell population. We also note the significant upregulation of *Col1a2*, a major component of vascular wall. Loss of *Col1a2* is associated with vasculopathy and aortic dilation.[43] This suggests that pulsatility of stretch likely drives other EC contributions to the structure of the arterial wall—and arterial vascular identity—beyond the recruitment of vSMCs.

While all cell types present in blood vessels experience hemodynamic force to some degree, our study focuses on the endothelium as a primary force sensor for the vessel for several reasons. First, from a developmental perspective, blood vessels are initially formed by the differentiation of angioblasts into ECs, and initial vessels are shaped by physical forces from by blood flow on ECs.[44] Second, most vascular malformations are driven by mutations in ECs that impact proliferation.[45] As the endothelium is in immediate contact with the bloodstream, ECs are a logical and attractive primary target for therapeutic drug delivery. Third, after vessels form, ECs are the only cell layer subject to force in all three dimensions, making them an excellent candidate first responder to force. While smooth muscle also senses stretch, it instead aligns perpendicular to stretch, and does not experience shear stress *in vivo*.[46] Of note, it also does not secrete PDGFB.

Future studies will be necessary to investigate the responses of vascular smooth muscle to pulsatile stretch.

While we focused on the paracrine signaling of EC-derived PDGFB to vSMCs, we also noted the upregulation of CX3CL1 in pulsatile-stretched HPAECs. CX3CL1 is a well-known chemokine that increases leukocyte recruitment and adhesion to endothelial cells.[47,48] The role of the immune system in the vascular complications of Glenn circulation is a wholly unappreciated factor; however, previous work in hereditary AVMs identified accumulation of leukocytes in brain AVMs and skin telangiectasias.[49-51] Collectively, these findings suggest that pulsatile stretch may impact EC-leukocyte cross-talk in pathogenesis of vascular malformations.

In summary, we show that the pulsatility of hemodynamic forces is sensed by the endothelium uniquely in each dimension of force, and through the sensing of pulsatile stretch secretes PDGFB to signal for support from vascular smooth muscle. The architecture and cellular composition of the vessel wall changes significantly upon loss of pulsatility in the Glenn, with thinning of the vascular wall, thereby shifting arterial structure toward that of a vein. Together, this work underscores the critical importance of proper blood flow dynamics for stability of vascular structure and function. In addition, it points to biomechanical signaling pathways as potential novel targets for therapeutic intervention in patients with pulsatility loss, such as in the Glenn circulation. We seek to better understand and address the mechanistic underpinnings of vascular defects that occur during single ventricle palliation, and anticipate that our data on pulsatility will provide the foundation for improving clinical outcomes for children that undergo these necessary surgeries.

ACKNOWLEDGEMENTS

We are grateful to the entire Cleaver Lab for useful discussions and reading of the manuscript. We thank Denise Marciano for the use of her lab's Flexcell apparatus. The results here are in part based upon data generated by the LungMAP Consortium and downloaded from (www.lungmap.net), on March 15, 2025. The LungMAP consortium, the Human Tissue Core (U01-HL144861), and the LungMAP Data Coordinating Center (U24-HL148865) are funded by the National Heart, Lung, and Blood Institute (NHLBI).

Author contributions

Conceptualization: S.S., T.H., M.F., O.C.; Methodology: S.S., T.H., M.F., S.R., A.D.S., O.C.; Investigation: S.S., L.T., T.W., S.R., O.C.; Resources: S.S., T.W., A.D.S., T.C., O.C.; Data curation: S.S., M.A.C., L.T., T.H.; Writing - original draft: S.S., O.C.; Writing - review & editing: S.S., T.H., A.D.S., O.C.; Visualization: M.A.C., S.S.; Supervision: S.S., O.C.; Project administration: S.S., O.C.; Funding acquisition: S.S., T.C., A.D.S., O.C.

Funding

This research was supported in part by grants from the American Thoracic Society/Alveolar Capillary Dysplasia (ACDMPV) Research Grant (23-24PACDA12 to S.S.); National Heart Lung and Blood Institute (HL113498 to O.C., K08HL157510 to ADS; the National Academy of Science, Engineering, and Medicine Ford Foundation Dissertation Fellowship (M.A.C.); and the Foundation Leducq grant (21CVD03 to O.C.).; National Institutes of Health (R01DK127634, RC2 DK125960 to T.C.) and Cancer Prevention Research Institute of Texas (RP220201 to T.C.). Open Access funding provided by University of Texas Southwestern Medical Center. Deposited in PMC for immediate release.

712 **REFERENCES**
713

714 1. Spearman, A.D. & Ginde, S. Pulmonary Vascular Sequelae of Palliated Single Ventricle
715 Circulation: Arteriovenous Malformations and Aortopulmonary Collaterals. *Journal of*
716 *Cardiovascular Development and Disease* **9**, 309 (2022).
717 2. Srivastava, D.*, et al.* Hepatic venous blood and the development of pulmonary
718 arteriovenous malformations in congenital heart disease. *Circulation* **92**, 1217-1222
719 (1995).
720 3. McElhinney, D.B.*, et al.* Incorporation of the hepatic veins into the cavopulmonary
721 circulation in patients with heterotaxy and pulmonary arteriovenous malformations
722 after a Kawashima procedure. *Ann Thorac Surg* **80**, 1597-1603 (2005).
723 4. Shah, M.J., Rychik, J., Fogel, M.A., Murphy, J.D. & Jacobs, M.L. Pulmonary AV
724 Malformations After Superior Cavopulmonary Connection: Resolution After Inclusion
725 of Hepatic Veins in the Pulmonary Circulation. *The Annals of Thoracic Surgery* **63**, 960-
726 963 (1997).
727 5. Kurotobi, S.*, et al.* Bidirectional cavopulmonary shunt with right ventricular outflow
728 patency: The impact of pulsatility on pulmonary endothelial function. *The Journal of*
729 *thoracic and cardiovascular surgery* **121**, 1161-1168 (2001).
730 6. Henaine, R.*, et al.* Hemodynamics and arteriovenous malformations in cavopulmonary
731 anastomosis: the case for residual antegrade pulsatile flow. *The Journal of thoracic and*
732 *cardiovascular surgery* **146**, 1359-1365 (2013).
733 7. Sakaki, M.*, et al.* Pulmonary function in a non-pulsatile pulmonary circulation. *ASAIO J*
734 **38**, M366-369 (1992).
735 8. Buschmann, I.*, et al.* Pulsatile shear and Gja5 modulate arterial identity and remodeling
736 events during flow-driven arteriogenesis. *Development* **137**, 2187-2196 (2010).
737 9. Simons, M. & Eichmann, A. Molecular controls of arterial morphogenesis. *Circ Res* **116**,
738 1712-1724 (2015).
739 10. McEvoy, E.*, et al.* Feedback between mechanosensitive signaling and active forces
740 governs endothelial junction integrity. *Nat Commun* **13**, 7089 (2022).
741 11. Dessalles, C.A., Leclech, C., Castagnino, A. & Barakat, A.I. Integration of substrate- and
742 flow-derived stresses in endothelial cell mechanobiology. *Commun Biol* **4**, 764 (2021).
743 12. Kutys, M.L. & Chen, C.S. Forces and mechanotransduction in 3D vascular biology. *Curr*
744 *Opin Cell Biol* **42**, 73-79 (2016).
745 13. Chavkin, N.W.*, et al.* Endothelial cell cycle state determines propensity for arterial-
746 venous fate. *Nat Commun* **13**, 5891 (2022).
747 14. Trimm, E. & Red-Horse, K. Vascular endothelial cell development and diversity. *Nat Rev*
748 *Cardiol* **20**, 197-210 (2023).
749 15. Lindahl, P., Johansson, B.R., Leveen, P. & Betsholtz, C. Pericyte loss and microaneurysm
750 formation in PDGF-B-deficient mice. *Science* **277**, 242-245 (1997).
751 16. Hellstrom, M., Kalen, M., Lindahl, P., Abramsson, A. & Betsholtz, C. Role of PDGF-B and
752 PDGFR-beta in recruitment of vascular smooth muscle cells and pericytes during
753 embryonic blood vessel formation in the mouse. *Development* **126**, 3047-3055 (1999).
754 17. Lin, Y.*, et al.* Role of endothelial PDGFB in arterio-venous malformations pathogenesis.
755 *Angiogenesis* **27**, 193-209 (2024).
756 18. Uebelhoer, M.*, et al.* Venous malformation-causative TIE2 mutations mediate an AKT-
757 dependent decrease in PDGFB. *Hum Mol Genet* **22**, 3438-3448 (2013).

758 19. Malek, A.M., Gibbons, G.H., Dzau, V.J. & Izumo, S. Fluid shear stress differentially
759 modulates expression of genes encoding basic fibroblast growth factor and platelet-
760 derived growth factor B chain in vascular endothelium. *J Clin Invest* **92**, 2013-2021
761 (1993).
762 20. Sumpio, B.E.*, et al.* Regulation of PDGF-B in endothelial cells exposed to cyclic strain.
763 *Arterioscler Thromb Vasc Biol* **18**, 349-355 (1998).
764 21. Velasco Forte, M.N.*, et al.* MRI for Guided Right and Left Heart Cardiac Catheterization:
765 A Prospective Study in Congenital Heart Disease. *J Magn Reson Imaging* **53**, 1446-1457
766 (2021).
767 22. Guo, M.*, et al.* Guided construction of single cell reference for human and mouse lung.
768 *Nat Commun* **14**, 4566 (2023).
769 23. Gaddis, N.*, et al.* LungMAP Portal Ecosystem: Systems-level Exploration of the Lung. *Am*
770 *J Respir Cell Mol Biol* **70**, 129-139 (2024).
771 24. Wan, T.C.*, et al.* Glenn circulation causes early and progressive shunting in a surgical
772 model of pulmonary arteriovenous malformations. *Physiol Rep* **12**, e70123 (2024).
773 25. Lim, H.S. & Gustafsson, F. Pulmonary artery pulsatility index: physiological basis and
774 clinical application. *Eur J Heart Fail* **22**, 32-38 (2020).
775 26. Deng, H., Eichmann, A. & Schwartz, M.A. Fluid Shear Stress-Regulated Vascular
776 Remodeling: Past, Present, and Future. *Arterioscler Thromb Vasc Biol* (2025).
777 27. Corada, M., Morini, M.F. & Dejana, E. Signaling pathways in the specification of arteries
778 and veins. *Arterioscler Thromb Vasc Biol* **34**, 2372-2377 (2014).
779 28. Resnick, N.*, et al.* Platelet-derived growth factor B chain promoter contains a cis-acting
780 fluid shear-stress-responsive element. *Proc Natl Acad Sci U S A* **90**, 4591-4595 (1993).
781 29. Gray, R.G.*, et al.* Persistent antegrade pulmonary blood flow post-glenn does not alter
782 early post-Fontan outcomes in single-ventricle patients. *Ann Thorac Surg* **84**, 888-893;
783 discussion 893 (2007).
784 30. Chen, Q.*, et al.* Does the persistence of pulsatile antegrade pulmonary blood flow
785 following bidirectional Glenn procedure affect long term outcome? *Eur J Cardiothorac*
786 *Surg* **47**, 154-158; discussion 158 (2015).
787 31. Kowatari, R., Suzuki, Y., Daitoku, K. & Fukuda, I. Long-term results of additional
788 pulmonary blood flow with bidirectional cavopulmonary shunt. *J Cardiothorac Surg* **15**,
789 279 (2020).
790 32. Berdat, P.A., Belli, E., Lacour-Gayet, F., Planche, C. & Serraf, A. Additional pulmonary
791 blood flow has no adverse effect on outcome after bidirectional cavopulmonary
792 anastomosis. *Ann Thorac Surg* **79**, 29-36; discussion 36-27 (2005).
793 33. van de Wal, H.J.C.M.*, et al.* Bi-directional cavopulmonary shunt: is accessory pulsatile
794 flow, good or bad? *European Journal of Cardio-Thoracic Surgery* **16**, 104-110 (1999).
795 34. Ferns, S.J.*, et al.* Is additional pulsatile pulmonary blood flow beneficial to patients with
796 bidirectional Glenn? *The Journal of thoracic and cardiovascular surgery* **145**, 451-454
797 (2013).
798 35. Uemura, H.*, et al.* Use of the bidirectional Glenn procedure in the presence of forward
799 flow from the ventricles to the pulmonary arteries. *Circulation* **92**, II228-232 (1995).
800 36. Januszewska, K., Nawrocki, P., Bruenen, A., Schnabel, A. & Malec, E. Significance of
801 additional pulmonary blood flow between second and third stage in Fontan pathway.
802 *BMC pediatrics* **24**, 705 (2024).

803 37. Shikata, Y., *et al.* Differential effects of shear stress and cyclic stretch on focal adhesion
804 remodeling, site-specific FAK phosphorylation, and small GTPases in human lung
805 endothelial cells. *Exp Cell Res* **304**, 40-49 (2005).
806 38. Birukova, A.A., *et al.* Differential regulation of pulmonary endothelial monolayer
807 integrity by varying degrees of cyclic stretch. *Am J Pathol* **168**, 1749-1761 (2006).
808 39. Hays, B.S., *et al.* Histopathological abnormalities in the central arteries and veins of
809 Fontan subjects. *Heart (British Cardiac Society)* **104**, 324-331 (2018).
810 40. Lammers, S., *et al.* Mechanics and Function of the Pulmonary Vasculature: Implications
811 for Pulmonary Vascular Disease and Right Ventricular Function. in *Comprehensive*
812 *Physiology* 295-319 (2012).
813 41. Townsley, M.I. Structure and composition of pulmonary arteries, capillaries, and veins.
814 *Compr Physiol* **2**, 675-709 (2012).
815 42. Van Gieson, E.J., Murfee, W.L., Skalak, T.C. & Price, R.J. Enhanced Smooth Muscle Cell
816 Coverage of Microvessels Exposed to Increased Hemodynamic Stresses In Vivo.
817 *Circulation Research* **92**, 929-936 (2003).
818 43. Takeda, R., *et al.* Clinical and molecular features of patients with COL1-related
819 disorders: Implications for the wider spectrum and the risk of vascular complications.
820 *Am J Med Genet A* **188**, 2560-2575 (2022).
821 44. Lucitti, J.L., *et al.* Vascular remodeling of the mouse yolk sac requires hemodynamic
822 force. *Development* **134**, 3317-3326 (2007).
823 45. Nguyen, H.L., Boon, L.M. & Vikkula, M. Vascular Anomalies Caused by Abnormal
824 Signaling within Endothelial Cells: Targets for Novel Therapies. *Semin Intervent Radiol*
825 **34**, 233-238 (2017).
826 46. Wang, J.H., Goldschmidt-Clermont, P., Wille, J. & Yin, F.C. Specificity of endothelial cell
827 reorientation in response to cyclic mechanical stretching. *J Biomech* **34**, 1563-1572
828 (2001).
829 47. Lesnik, P., Haskell, C.A. & Charo, I.F. Decreased atherosclerosis in CX3CR1−/− mice
830 reveals a role for fractalkine in atherogenesis. *Journal of Clinical Investigation* **111**,
831 333-340 (2003).
832 48. Bazan, J.F., *et al.* A new class of membrane-bound chemokine with a CX3C motif. *Nature*
833 **385**, 640-644 (1997).
834 49. Chen, Y., *et al.* Evidence of Inflammatory Cell Involvement in Brain Arteriovenous
835 Malformations. *Neurosurgery* **62**, 1340-1350 (2008).
836 50. Zhang, R., *et al.* Persistent infiltration and pro-inflammatory differentiation of
837 monocytes cause unresolved inflammation in brain arteriovenous malformation.
838 *Angiogenesis* **19**, 451-461 (2016).
839 51. Braverman, I.M., Keh, A. & Jacobson, B.S. Ultrastructure and three-dimensional
840 organization of the telangiectases of hereditary hemorrhagic telangiectasia. *J Invest*
841 *Dermatol* **95**, 422-427 (1990).
842

SUPPLEMENTARY DATA

SUPPLEMENTARY FIGURES

Supplemental Fig 1: Comparison of arterial and venous characteristics highlights the definitional importance of pulsatility

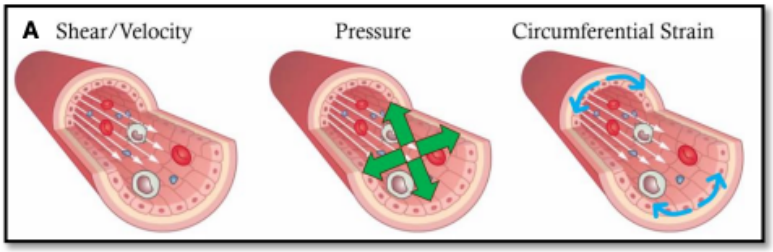

B		Systemic		Pulmonary		Umbilical	
		Artery	Vein	Artery	Vein	Artery	Vein
Hemodynamic Forces	Pulsatility	YES	NO	YES	NO	YES	NO
	Mean Pressure (mm Hg)	70	4	12	6	50	20
	Peak Velocity (cm/s)	100	15	75	40	45	15
Gas Transport	PO2	100	40	40	100	20	30
	PCO2	40	45	45	40	50	40
	pH	7.4	7.36	7.36	7.4	7.27	7.35
	Hgb Saturation	100%	70%	70%	100%	50%	70%
	Hgb Isoforms	HgbA/B	HgbA/B	HgbA/B	HgbA/B	HgbF	HgbF
Histological Features	Intima	+	+	+	+	+	+
	Internal Elastic Lamina	++	+	++	+	-	-
	Media (VSMCs)	+++	+	+++	+	+++	+
	Adventitia	++	+	++	+	++	+
	Forms Valves	NO	YES	NO	NO	NO	NO

Supplemental Figure 1: Comparison of arterial and venous characteristics highlights the definitional importance of pulsatility. a Three dimensions of hemodynamic force on endothelial cells. **b** Comparison of key features of the three major anatomical sets of arteries and veins. Pulsatility is common to all arteries despite their pressure, oxygenation, or peak shear stress/velocity.

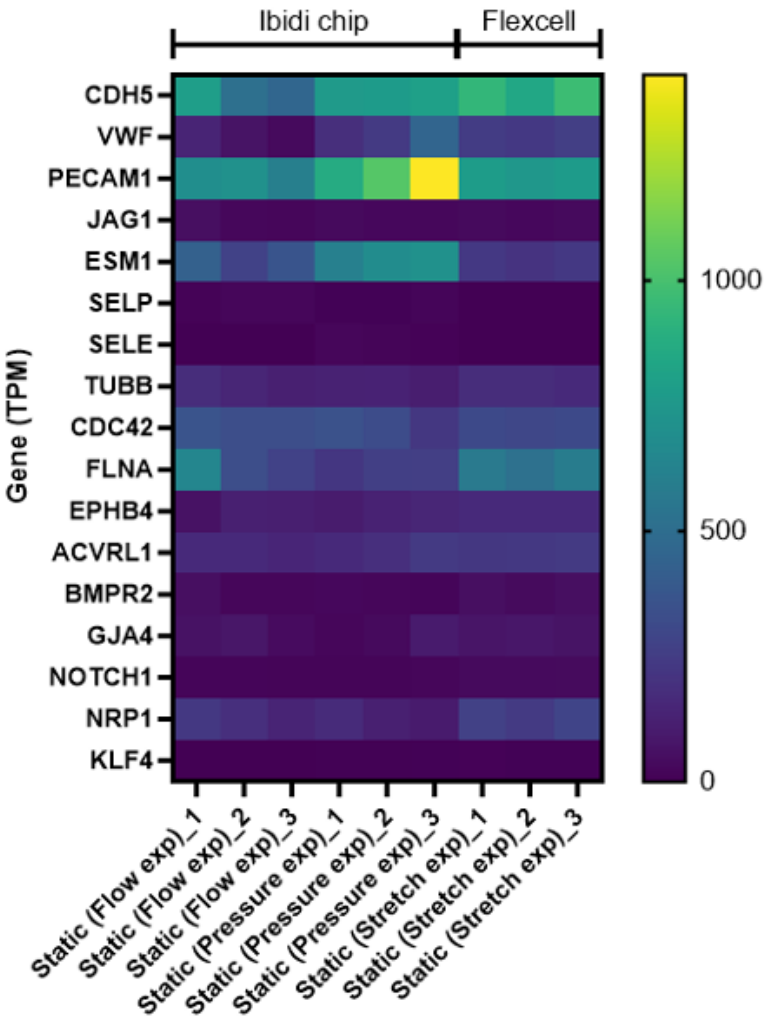

Supplemental Figure 2: Comparison of baseline transcriptome of key endothelial genes under static conditions. Heatmap comparing baseline expression of key endothelial cell genes shows that despite being seeded on different substrates, endothelial cells used in our experiments did not vary in their baseline conditions prior to the application of pulsatile or non-pulsatile force.

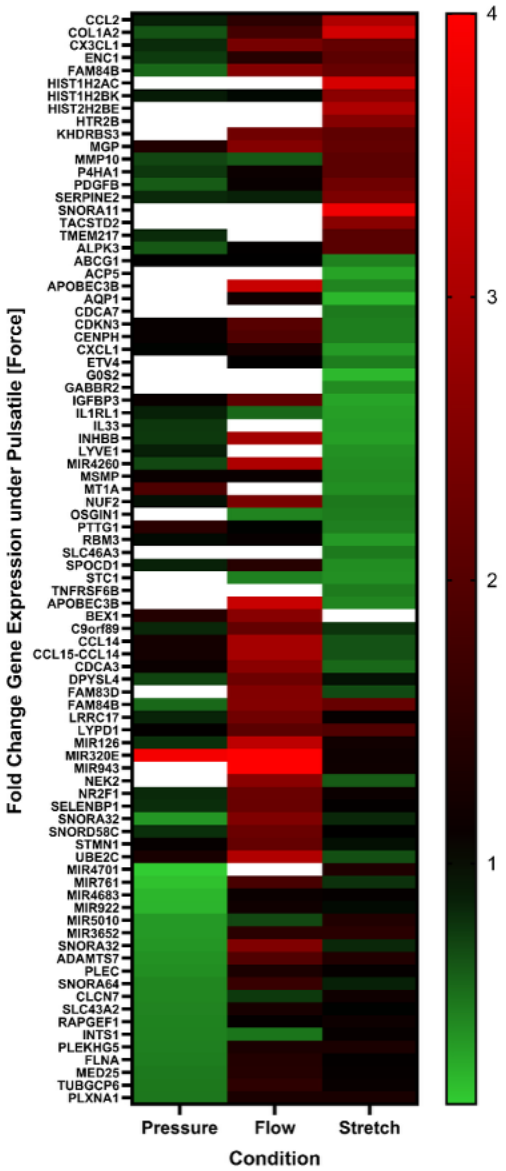

Supplemental Figure 3: Impact of pulsatility on significantly regulated genes. Comparison of all significantly regulated genes in figure 3, showing fold change in gene expression under different dimensions of force, comparing pulsatile to non-pulsatile conditions. White boxes indicate gene was excluded from analysis for that condition due to low expression (TPM < 10 for that gene under both pulsatile and non-pulsatile conditions).

SUPPLEMENTARY TABLES

	Glenn	Controls
Demographics	n = 20	n = 17
Age in years	4.4 (1.5)	4.5 (0.9)
Male	12 (60%)	8 (90%)
Cardiac Diagnosis		
Single ventricle - Glenn stage	20 (100%)	
Systemic left ventricle	9 (45%)	17 (100%)
Heart Transplantation		9
Atrial septal defect		4
Coarctation of the aorta		2
Bicuspid aortic valve		1
Ebsteins Anomaly		1
Hemodynamic State		
Cardiac Index	4.1 (0.5)	2.8 (0.5)

Supplemental Table 1: Patient Demographics. Descriptive statistics of patient data included in the study. Data is presented as mean (standard deviation) unless otherwise noted.

max	min	mean	PD	PI
20	5	10	**15**	**1.5**
30	5	16.2	**25**	**1.5**
40	10	20	**30**	**1.5**
50	15	23	**35**	**1.5**

Supplemental Table 2: Comparison of Pulsatility Index and Pulse Difference. Comparison of pulsatility index (PI) and pulse difference (PD) shows that PI can be unchanged for a variety of different PD.